SUPPLEMENTAL MATERIALS ACCOMPANYING MANUSCRIPT:

IN VITRO 3D PHENOTYPIC DRUG SCREEN IDENTIFIES CELASTROL AS AN EFFECTIVE IN VIVO INHIBITOR OF POLYCYSTIC KIDNEY DISEASE

Tijmen H. Booij[1,2#], Wouter N. Leonhard[3#], Hester Bange[4], Kuan Yan[4], Michiel Fokkelman[1], Anna J. Plugge[3], Kimberley A.M. Veraar[3], Johannes G. Dauwerse[3], Gerard J.P. van Westen[5], Bob van de Water[1], Leo S. Price[1,4¥], Dorien J.M. Peters[3¥*].

# Authors contributed equally
¥ Authors contributed equally
* Corresponding author

Author Affiliation
[1]Division of Toxicology, Leiden Academic Centre for Drug Research (LACDR), Leiden University, Leiden, The Netherlands
[2]NEXUS Personalized Health Technologies, ETH Zürich, Switzerland
[3]Department of Human Genetics, Leiden University Medical Center (LUMC), Leiden, The Netherlands
[4]OcellO B.V., Leiden, The Netherlands
[5]Division of Medicinal Chemistry, Leiden Academic Centre for Drug Research (LACDR), Leiden, The Netherlands

Short Title
Celastrol to treat PKD

Corresponding Author
Dorien J.M. Peters, Prof. Dr.
Department of Human Genetics
Leiden University Medical Center (LUMC)
P.O. Box 9600
2300 RC Leiden
The Netherlands
+31 715269490
d.j.m.peters@lumc.nl

Keywords
PKD, celastrol, pyrvinium pamoate, high-content screening, 3D

Classification
Biological Sciences/Medical Sciences

Supplemental Methods

Cell lines and maintenance

mIMCD3 sh*Pkd1* cells, with a short-hairpin mediated knockdown of *Pkd1*, and mIMCD3 *Pkd1*$^{-/-}$, an RNA-guided FokI nuclease-mediated *Pkd1* knockout cell line (mIMRFNPKD clone 5E4), were generated previously (1) and maintained in DMEM/F12 (Ham's) culture medium (D8062, Sigma Aldrich, Zwijndrecht, Netherlands), supplemented with 10% fetal bovine serum (FBS, obtained from Gibco Fisher Scientific, Landsmeer, Netherlands), glutamax and penicillin/streptomycin in 175cm^2 culture flasks (Corning). Before reaching maximal confluence, the monolayers were washed with 1x PBS (Sigma Aldrich, Zwijndrecht, Netherlands) and subsequently trypsinized with 1x Trypsin (Gibco Fisher Scientific, Landsmeer, Netherlands) and subsequently passaged to a new culture flask. Cell passage numbers were kept below 20 for all experiments. For cryopreservation, trypsinized cells were pelleted by centrifugation at 1500rpm for 5 minutes and the cell pellet was subsequently mixed with freezing medium consisting of 90% FBS and 10% DMSO (Biosolve B.V., Valkenswaard, Netherlands) at a concentration of 9*10^6 cells per mL and subsequently slow-frozen to -150°C.

3D cyst culture procedure

mIMCD3 sh*Pkd1* or mIMCD3 *Pkd1*$^{-/-}$ cells were quick-thawed and cultured in 175cm^2 culture flasks 72 hours prior to initiation of the 3D cultures. 3D cyst cultures were prepared as described previously (1). Briefly, cells were trypsinized and subsequently pelleted by centrifugation. The cell pellet was mixed with Cyst-Gel (OcellO B.V. Leiden, Netherlands) at a cell density of 3*10^6 cells per mL. Using a CyBio Selma 96 or CyBio Felix automated liquid handler (Analytik Jena AG, Jena, Germany), cell-gel mix was transferred to Greiner µClear 384 well plates (Greiner Bio-One B.V. Alphen aan den Rijn, Netherlands), 14.5µL per well, at a final cell density of 2175 cells per well. After 30 minutes of gel polymerization at 37°C, 33.5µL culture medium was added and cells were grown for 72 hours (mIMCD3 sh*Pkd1* cells) or 96 hours (mIMCD3 *Pkd1*$^{-/-}$) at 37°C (5% CO_2) to initiate lumen formation, prior to compound exposures. Subsequently, cells were co-exposed with 2.5µM forskolin (*Coleus forskohlii*, Calbiochem, Millipore B.V., Amsterdam, Netherlands), to enhance cyst swelling due to the activation of adenylyl cyclase to produce cAMP, and compounds, using either the CyBio Selma 96 or Felix (for smaller scale experiments), or, to screen compound libraries, a BioMek FXP (Beckman Coulter B.V., Woerden, Netherlands) equipped with a 96-tip pipetting head. After 72 hours of compound exposures, plates were fixed with 4% formaldehyde (Sigma Aldrich, Zwijndrecht, Netherlands), permeabilized with Triton X-100 (Sigma Aldrich, Zwijndrecht, Netherlands) and stained with rhodamine-phalloidin (Sigma Aldrich, Zwijndrecht, Netherlands) and Hoechst 33258 (Sigma Aldrich, Zwijndrecht, Netherlands) for cytoskeleton and nuclei, respectively, for 12 to 24 hours at 4°C. After fixation and staining, plates were washed with 1x PBS for 24 hours and sealed with an aluminium plate seal (Greiner Bio-One B.V. Alphen aan den Rijn, Netherlands) and subsequently stored at 4°C prior to imaging (the screening procedure is schematically presented in supplemental figure S1).

Long-term 3D cyst culture procedure without forskolin

3D cyst cultures of mIMCD3 *Pkd1*$^{-/-}$ cells were prepared as described in the previous section. 33.5µL of culture medium was added to the prepared cultures, and cells were allowed to form cysts for 96 hours prior to compound exposures. 3D cultured cysts were exposed to 100nM celastrol or solvent (0.1% DMSO) in a final volume of 60µL. After 96 hours, 30µL medium/compound mix was aspirated using a CyBi Selma 96, and 18µL fresh medium and

2x 6µL fresh compound was added. After 96 hours, the cysts were fixed with 4% formaldehyde and further processed as described above.

Compounds
A (SPECTRUM) compound library with 2320 molecules was obtained from MicroSource (MicroSource Discovery Systems, Inc., Gaylordsville, Connecticut, USA). Compounds were pre-dissolved to 10mM in DMSO. Analytical grade DMSO was obtained from Biosolve B.V. (Valkenswaard, Netherlands). Rapamycin, sorafenib tosylate, roscovitine, tolvaptan and NVP-BEZ-235 were obtained from SelleckChem (Munich, Germany). Metformin HCl was obtained from Sigma Aldrich (Zwijndrecht, Netherlands). Celastrol was obtained from two different sources (MicroSource Discovery Systems, Inc., Gaylordsville, Connecticut, USA for the primary screen and Sigma Aldrich, Zwijndrecht, Netherlands for further validation experiments and animal experiments). Both sources performed equally well in terms of cyst growth inhibition *in vitro* (not shown).

Fluorescence microscopy
384 well plates of the SPECTRUM screen were imaged using an automated (wide-field) BD Pathway 855 imager (BD Biosciences, Breda, Netherlands) with a 4x Olympus objective, coupled to a Twister II robotic arm, as described previously (2). Subsequent experiments were imaged using an ImageXpress Micro XLS wide field high-content analysis system (Molecular Devices, Sunnyvale, CA, USA) with a 4x objective. *xy*-images were made in the *z*-direction for each well, requiring approximately 25 images for each well. Images captured with the BD pathway microscope captured approximately 70% of each well, whereas images made with the ImageXpress imager could capture the entire well.

Image- and data analysis
Image stacks for each well were analysed and phenotypes were quantified as described previously (1), using Ominer software integrated in KNIME Analytics Platform (KNIME version 3.1.2, Konstanz, Germany, http://www.knime.org/). 450 phenotypic measurements were *z*-score normalized to plate median, or normalized to percent of control (100% corresponding with forskolin-stimulated control median and 0% with unstimulated/vehicle control median). For heatmap plots of efficacy, data was scaled between 0% inhibition of cyst growth (forskolin-stimulated control median) and 100% inhibition (unstimulated control median) for presentation purposes. Linear discriminant analysis (LDA) for the validation screen was performed using an R script (https://www.r-project.org/) integrated in KNIME. In order to remove most highly correlating phenotypic parameters prior to training the LDA, we applied a correlation filter (Pearson product-moment correlation coefficient <0.85 or >-0.85) to all 450 phenotypic parameters to filter out the 367 most highly correlating parameters. The LDA model was subsequently trained based on unstimulated control (solvent, 0.2% DMSO), stimulated control (2.5µM forskolin) and known cytotoxic molecules in the library (epirubicin, doxorubicin, daunorubicin, staurosporin and gambogic acid, at 1µM concentration) and thereafter applied to all data, yielding two linear discriminants, linear discriminant 1 (LD1) and linear discriminant 2 (LD2). Linear discriminants were thereafter scaled from 0 to 100% (labelled % efficacy and % toxicity for LD1 and LD2, respectively, for presentation purposes). The phenotypic descriptors and their coefficients that were included in the linear discriminants are presented in supplemental table S1 (top 10 ranked features only). While LD1 strongly separated unstimulated (0.2% DMSO) controls from stimulated controls (2.5µM forskolin), LD2 exclusively discriminated (un)stimulated conditions from known toxic molecules. The absolute distance to the unstimulated control group for all data points was calculated based on these scaled linear discriminants and

presented as a heatmap plot using the ggplot2 package (http://ggplot2.org) for Rstudio 0.99.878 (https://www.rstudio.com/products/rstudio2) with R3.2.3 (https://www.r-project.org/). S-curve plots were made using the ggplot2 package. 3D scatterplots presented in the supplemental figures were generated with the Scatterplot3D package (https://CRAN.R-project.org/package=scatterplot3d)(3) in R3.2.3. Density plots were generated with ggplot2 for R and other charts were generated with Graphpad Prism 7 (Graphpad Software, La Jolla, California, USA).

Animal procedures

The local animal experimental committee of the Leiden University Medical Center (LUMC) and the Commission Biotechnology in Animals of the Dutch Ministry of Agriculture approved all animal experiments performed. Experiments were done in conformity with EU Directive 2010/63/EU 'On the protection of animals for experimental and other scientific purposes'.

To assess the efficacy of celastrol *in vivo* we used kidney–specific, tamoxifen–inducible Cre-*Pkd1*lox mice (iKspCre-*Pkd1*^{lox,lox}) (4, 5). To inactivate the *Pkd1* gene, mice received 15mg/kg Tamoxifen (in 1% ethanol in sunflower oil, dissolved by sonication) by oral gavage at post-natal day (P)10 and P11. From P13-P27, mice received intraperitoneal injections (i.p.) of either celastrol, pyrvinium pamoate (PP) or vehicle (5% DMSO + 10% Kolliphor EL in phosphate buffered saline). After the last injection at P27, blood samples were collected from the tail vein to assess the Blood Urea levels using Reflotron Technology and then the mice were euthanized by cervical dislocation. Kidneys were cut in halves and either snap frozen in liquid nitrogen or fixed in buffered 4% formaldehyde solution for embedding in paraffin. Total image scans of Periodic acid–Schiff (PAS) stained kidney sections (4µm) were processed semi-automatically using Photoshop software by an investigator who was blinded to the treatment, as done previously (6). Briefly, a specifically designed colour palette was used for all images to remove all pixels from the lumens/cysts, leaving only the pixels of the actual tissue. From these numbers, the percentage of 'cystic' pixels versus total number of pixels was calculated and defined as the cystic index.

Fibrotic index

The fibrotic index was calculated as done previously on the basis of Sirius Red staining (6). Briefly, tissue sections were stained after deparaffinization with 0.2% phosphomolybdic acid for 1 minute and 0.1% Sirius Red (in picric acid) for 90 minutes. This was followed by saturated picric acid and subsequently by ethanol/xylol wash step. Adobe Photoshop (Adobe Systems, Inc. San Jose, California, USA) was used for the quantification of Sirius Red.

Immunohistochemistry on 3D cyst cultures and tissue sections

Samples were subjected by O/N formaldehyde fixation (in buffered 4% formaldehyde solution) and embedded in paraffin. For immunohistochemical analysis, 4µm sections were deparaffinised and subjected to heat-mediated antigen retrieval (10mM/1mMTris/
EDTA) [pH 9.0] for anti-p (Tyr705) STAT3 [no. 9145; Cell Signaling Technology], and 10 mM citrate buffer [pH 6.0] for anti–Ki-67 [no. NCL-Ki67p; Bio Connect Services] anti-phospho-CREB [Ser133], anti-phospho-ERK1/2 [Thr202/204], anti-phospho-ribosomal protein S6 (Ser240/244) from Cell Signaling Technology (no's. 9198, 4370 and 2215 respectively) and anti-Na^+/K^+-ATPase (ab76020, Abcam). Sections were blocked with 0.1% H_2O_2 for 20 min for endogenous peroxidase activity and preincubated for 1 h with 5% normal goat serum in 1% BSA in PBS. Next, the sections were incubated O/N with anti-pSTAT3 (1:75), anti-p-rpS6 (1:100), anti-pERK1/2 (1:400), anti-Ki67 (1:3000), anti-Na^+/K^+-ATPase (1:6400) or anti-pCREB (1:800). After incubation with rabbit Envision horseradish

peroxidase (no. K4011; Dako) or rabbit anti-goat horseradish peroxidase (1:100; no. P0449; Dako), immune reactions were revealed using diaminobenzidine as a chromogen, counterstained with hematoxylin, dehydrated, and mounted.
For fluorescent immunohistochemistry, 1-hour incubation steps were used with anti-Na^+/K^+-ATPase (ab76020, Abcam) as the primary antibody (1:12800) and Alexa Fluor Goat anti-Rabbit-488 as the secondary antibody (1:200). The other steps were similar to those described for immunohistochemistry. Sections were then mounted using Prolong Gold (Thermofisher) including DAPI for regular nuclear staining.

Western blot and densitometric analysis
Half kidneys stored at -80°C were used to make protein extracts for analyses. Throughout the lysis procedure, 2 mM NaF, 1 mM Na2VO4, and protease inhibitor cocktail (Roche) were used to inhibit phosphatase and protease activity. Kidneys were homogenized in 600 µl RIPA without detergents (50mM Tris·HCl, pH 7.4, 150 mM NaCl, 1 mM EDTA) using Magnalyser technology (Roche) followed by three 5-s pulses of sonication. Next, an equal amount of RIPA with detergents (50 mM Tris·HCl, pH7.4, 150 mM NaCl, 1 mM EDTA, 2% DOC, 2% NP-40, 2% Triton X-100) was added and samples were incubated for 45 min at 4°C. Kidney lysates were spun-down for 10 min at 14,000 *g* and supernatants were stored at -80°C. 80–120 µg of kidney lysates was used for SDS-PAGE and immunoblotting. Membranes were blocked for 1 h in 25% sea block blocking buffer (Thermo Fisher Scientific/Pierce, no.37527) in PBS and incubated O/N with anti-pSTAT3 (1:1000), anti-p-rpS6 (1:2000), anti-pERK1/2 (1:2000), anti-Na^+/K^+-ATPase (1:10.000) or anti-α-Tubulin (1:2000, Calbiochem CP06) in 5% BSA-TBS (Tween 20, 0.1%). Goat-anti-rabbit (1:10000) DyLight 800 (Perbio Science, no.35571) was used as secondary antibody for the detection of anti-pSTAT3, anti-p-rpS6, and anti-pERK1/2, and goat-anti-mouse DyLight 680 (1:10000; Perbio Science, no.35518) was used as secondary antibody for the detection of anti-α-tubulin. Detection and densitometric analysis were carried out with the Odyssey Infrared Imaging System (Westburg).

qPCR
Following RNA isolation using standard procedures (Nucleospin kit, Bioke no. MN 740955) cDNA synthesis was performed using the Transcriptor First Strand cDNA Synthesis Kit (Roche). qPCR was performed on the LightCycler 480 II (Roche) using 2x FastStart SYBRGreen Master (Roche) using standard procedures. Data were analyzed with LightCycler 480 Software, version 1.5 (Roche). Relative gene expression levels were calculated using the delta-delta Ct method and normalization to Hprt expression. Mean gene expressions and SDs of the treatment groups were calculated. Primer sequences are available on request.

Proliferation index
Kidney sections were stained with anti-Ki67 (see section ‘Immunohistochemistry on 3D cyst cultures and tissue sections’) were scanned for further image analyses. Raw histology image sections were digitally enhanced and segmented using OcellO’s Ominer platform. Each individual nucleus was separated and extracted (figure 4D) from the enhanced images. The object extraction (or segmentation) was accomplished using Ominer’s proprietary segmentation algorithm designed for microtissue analysis. Nuclei were further classified into $Ki67^{+/-}$ by measuring the Ki67 staining strength. Digital background correction was performed on the raw Ki67 signal to eliminate staining variation between the outer medulla (OM) and cortex region before measuring the Ki67 staining strength. Furthermore, the final Ki67 staining strength is measured by the ratio between blue and red signal rather than pure

red signal. The choice is made based on the feature selection in the associated intensity measurements from a set of manually drawn ground truth ($Ki67^{+/-}$) nucleus masks.

Statistical analysis
Statistical analyses were performed in Graphpad Prism 7 software, using one-way ANOVA coupled to Dunnett's multiple comparison's adjustment unless otherwise stated. Results were considered statistically significant with $p<0.05$, and this is further annotated in figure legends.

References Belonging to Supplemental Methods

1. Booij TH, et al. (2017) High-throughput phenotypic screening of kinase inhibitors to identify drug targets for polycystic kidney disease. *SLAS Discov* 22(8):974-984.
2. Booij TH, et al. (2016) Development of a 3D Tissue Culture-Based High-Content Screening Platform That Uses Phenotypic Profiling to Discriminate Selective Inhibitors of Receptor Tyrosine Kinases. *J Biomol Screen* 21(9):912-922.
3. Ligges U, Mächler M (2003) Scatterplot3D - an R Package for Visualizing Multivariate Data. *J Stat Soft* 8(11):1-20.
4. Lantinga-van Leeuwen IS, et al. (2006) Transgenic mice expressing tamoxifen-inducible Cre for somatic gene modification in renal epithelial cells. *Genesis* 44(5):225-232.
5. Lantinga-van Leeuwen IS, et al. (2007) Kidney-specific inactivation of the Pkd1 gene induces rapid cyst formation in developing kidneys and a slow onset of disease in adult mice. *Hum Mol Genet* 16(24):3188-3196.
6. Leonhard WN, et al. (2016) Inhibition of activin signaling slows progression of polycystic kidney disease. *J Am Soc Nephrol* 27(12):3589-3599.

Supplemental Tables

Supplemental Table S1: Parameter contributions to LDA

LDA feature coefficients (top 10 negatively ranked)			
LD1		**LD2**	
Feature Name	**Interpretation**	**Feature Name**	**Interpretation**
nc.Mean(zernike_order_1_1).meas		nc.Mean(std_child_to_par_center_dist).corr.meas	(related to position of nuclei)
actin.Mean(lumen_avg_width).struct.meas	(lumen size)	actin.Mean(lumen_avg_width).struct.meas	(lumen size)
actin.Sum(area).meas	(cyst wall size)	nc.Mean(avg_child_to_par_boundary_dist).corr.meas	(related to position of nuclei)
actin.Mean(zernike_order_2_2).meas		actin.SD(child_count).corr.meas	
actin.Mean(axis_Ratio_Minor_Major).meas	(cyst wall shape related)	actin.Mean(zernike_order_2_2).meas	
nc.Sum(area).meas	(nuclear size)	org.SD(axis_Ratio_Minor_Major).meas	(cyst shape related)
actin.Mean(eccentricity).meas	(cyst wall shape related)	nc.SD(number_of_branches).meas	
org.Count*(area).meas	(number of cysts)	actin.Mean(eccentricity).meas	(cyst wall shape related)
nc.Mean(child_parent_size_ratio).corr.meas	(nuclear size relative to cyst)	nc.Sum(area).meas	(nuclear size)
nc.SD(maximum_intensity).meas		nc.Mean(solidity).meas	(nuclear roundness)

LDA feature coefficients (top 10 positively ranked)			
LD1	**LD2**	**LD1**	**LD2**
Feature Name	**Interpretation**	**Feature Name**	**Interpretation**
nc.Mean(maximum_intensity).meas	(staining intensity of nuclei)	nc.Mean(hu_order_1).meas	
org.Mean(number_of_single_junction_points).meas		actin.SD(eccentricity).meas	(cyst wall shape related)
nc.Mean(avg_child_to_par_boundary_dist).corr.meas	(related to position of nuclei)	org.Mean(axis_Ratio_Minor_Major).meas	(cyst shape related)
nc.Mean(number_of_end_points).meas		nc.SD(maximum_intensity).meas	(nuclear intensity)
nc.Mean(hu_order_1).meas		nc.SD(zernike_order_8_2).meas	
actin.Mean(std_intensity).meas	(actin intensity related)	actin.SD(child_parent_size_ratio).corr.meas	(related to thickness of cyst wall)
nc.SD(zernike_order_8_2).meas		actin.Mean(std_intensity).meas	(actin intensity related)
actin.SD(eccentricity).meas	(cyst wall shape related)	org.Mean(feret).meas	
nc.SD(ratio_Area_BoundingBox_Area).meas	(nuclear shape related)	actin.Sum(area).meas	(cyst wall size)
org.Mean(feret).meas	(cyst shape related)	nc.Mean(zernike_order_1_1).meas	

Supplemental Table S2: Pathways affected by celastrol

Pathways/Targets	Context	Pubmed ID	DOI
HIF-1, erythropoietin, VEGF, mTOR, P70S6K, eIF4E, Erk	Hepatocellular carcinoma	28242743	10.1124/mol.116.107706
NFκB	Acute hepatic dysfunction	28189063	10.1016/j.etap.2017.02.002
NOX2-derived ROS-dependent PP5-JNK signaling pathway	ROS induced neurodegenerative disorders	28129433	10.1111/jnc.13966
Lipid synthesis, Sirt1		28123944	10.1016/j.molmet.2016.11.002
Nrf2, Erk1/2, Nox2, Angiotensin II type 1 receptor		28119074	10.1016/j.ejphar.2017.01.027
IKKß		27931154	10.1080/13880209.2016.1241809
Cdc37, Annexin A2, eEF1A		27819370	10.1039/c6mb00691d
HSP90/Cdc37		27398312	10.1002/2211-5463.12081
NF-kappa B, MAPK, JAK/STAT and RANKL/OPG pathways	Autoimmune inflammation	27405485	10.1093/femspd/ftw059
IRAKs to block TLR4-mediated NFκB activation	Autoimmune inflammation	27181127	10.1016/S2095-4964(16)60257-1
miR-21/ERK	Cardiac fibrosis and cardiac dysfunction	27160852	10.1159/000445554
TLR4/MyD88/NFκB	Diabetic liver injury	27057550	10.1155/2016/2641248
AMPK/PGC1α/Sirt3	Diabetic myopathy and oxidative stress	27049825	10.3892/ijmm.2016.2549
miR-21/mTOR/p27	Gastric cancer	26500453	10.1186/s12935-015-0256-3
Autophagy		26473737	10.1371/journal.pone.0140745
HSP90		17010675	10.1016/j.ccr.2006.09.005
Calpain		18726991	10.1002/jcp.21565
hERG channel	Cancer	25866772	10.1155/2015/308475
Apoptosis mediated through mitochondrial dysfunction, Akt, PI3K, 4E-BP1, mTOR. Celastrol also inhibited the Akt/GSK3beta and Akt/NFκB survival pathways	Triple-negative breast cancer	25818165	10.1016/j.yexmp.2015.03.031
CYP1A2, CYP2C19, CYP2D6, CYP2E1 and CYP3A4		25811791	10.3109/00498254.2014.1003113
HIF-1 induction through ROS/Akt/p70S6K		25383959	10.1371/journal.pone.0112470
HSP90		24954307	10.1016/j.bbagen.2014.06.008
HIF-1α pathway by inhibition of mTOR/p70S6K/eIF4E and ERK1/2		24859482	10.3892/or.2014.3211
Cannabinoid receptory type 2	Neuropathic pain	25101848	10.3390/ijms150813637
NFκB	Inflammation	PMC4453024	10.5483/BMBRep.2015.48.3.147
Inhibit proteasome and upregulate *hsp30* and *hsp70* gene expression		20188206	10.1016/j.cbpa.2010.02.015
miR-21, PI3K/Akt, NFκB		24434352	doi: 10.1159/000357683
JNK, PTEN-Akt/mTOR pathway	Cadmium-induced neuronal cell death	24111524	10.1111/jnc.12474
Snail/E-cadherin	TGF-beta induced EMT	23850675	10.1016/j.bbrc.2013.06.113
Hsp70, Akt1, p70/S6K, ERK1/2	C2C12 myotube atrophy	23810294	10.1016/j.abb.2013.06.006
LOX-1	Atherosclerosis	23799016	10.1371/journal.pone.0065477
UDP-glucuronosyl transferase (UGT) 1A6 and 2B7		22669039	10.3390/molecules17066832
p-JNK, p-c-Jun, NFκB	Cerebral ischemia	22575561	10.1016/j.brainres.2012.04.054
Estrogen receptor α (ERα)	Breast cancer	20934245	10.1016/j.canlet.2010.09.006
Platelet activation (P-selectin and glycoprotein IIb/IIIa activation)		19661812	10.1097/FJC.0b013e3181b21472
VEGFR		18343027	10.1016/j.canlet.2008.01.043

Supplemental Figures

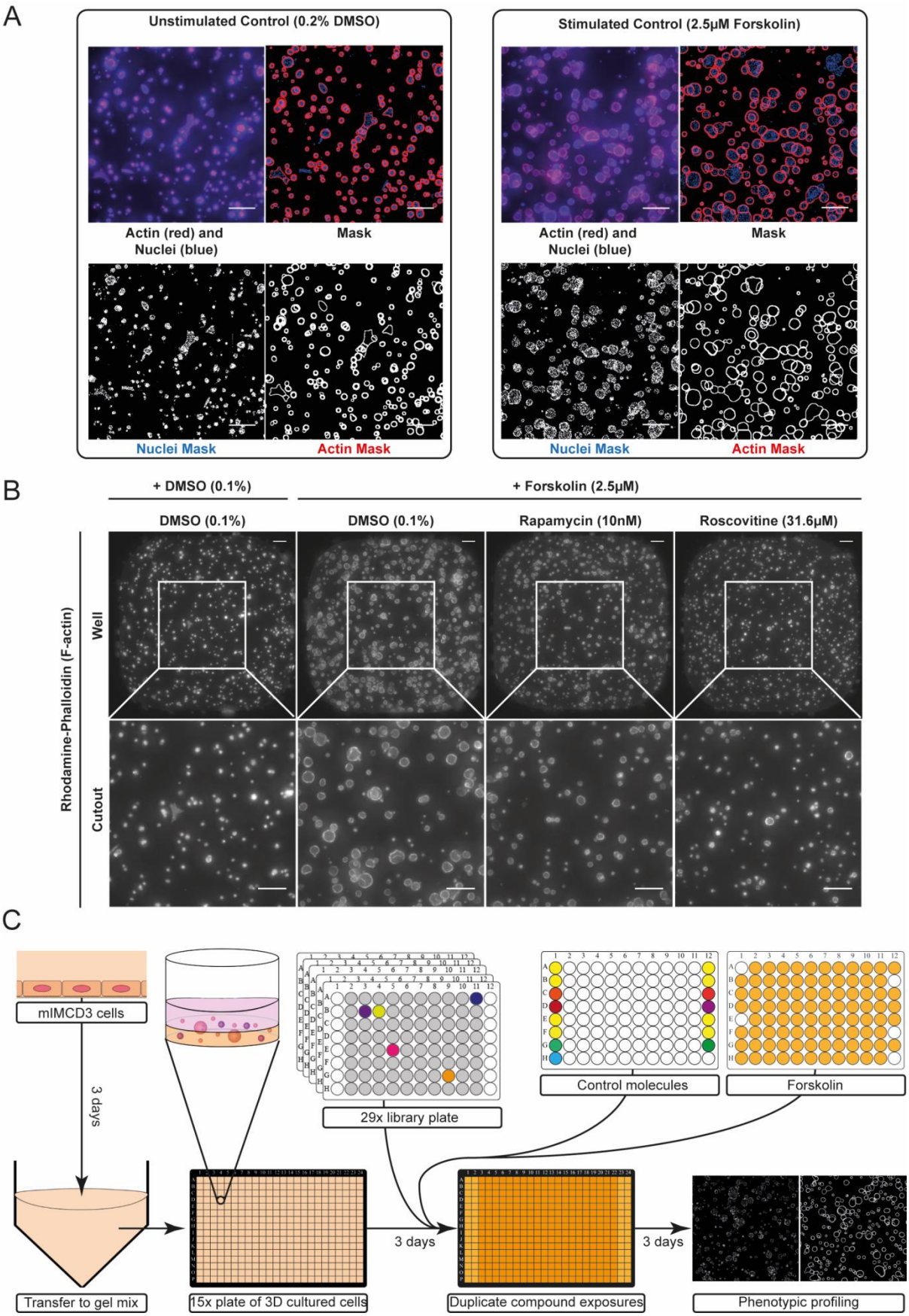

Supplemental figure S1: Screening molecule libraries using 3D cultured cysts. A) mIMCD3 *Pkd1*$^{-/-}$ cysts cultured for 96 hours in Cyst-Gel and exposed to solvent (unstimulated) or forskolin (stimulated). Image stacks of rhodamine-phalloidin and Hoechst 33258-stained cysts (top left images, brightness increased for presentation purposes) processed by Ominer software to generate- and quantify binary masks. 500x500px cut-out of the centre of the well shown. B) mIMCD3 *Pkd1*$^{-/-}$ cells were cultured for 96 hours in Cyst-Gel and exposed to solvent (DMSO) or control compounds (rapamycin, roscovitine) in the presence of forskolin. Cytoskeleton (F-actin) shown. Upper panel shows projected image stacks of entire well images with an ImageXpress micro XLS imager. Lower panel represents 500x500px cut-out of the centre of the well. Contrast and brightness enhanced for presentation purposes. B) Schematic representation of screening pipeline as described under supplemental methods. mIMCD3 sh*Pkd1* cells were mixed with Cyst-Gel and allowed to develop into small cysts during 72 hours, prior to exposure to the small molecule library. Control molecules were added to the outer plate columns, and forskolin was added to all wells, except for a few wells that served as 'unstimulated' controls (16 per plate). Staurosporin was added to the lower right corner of each plate to serve as positive control for cytotoxicity. After 72-hours incubation, cultures were stained, imaged and quantified as described in the supplemental methods section. Scale bars represent 250µm.

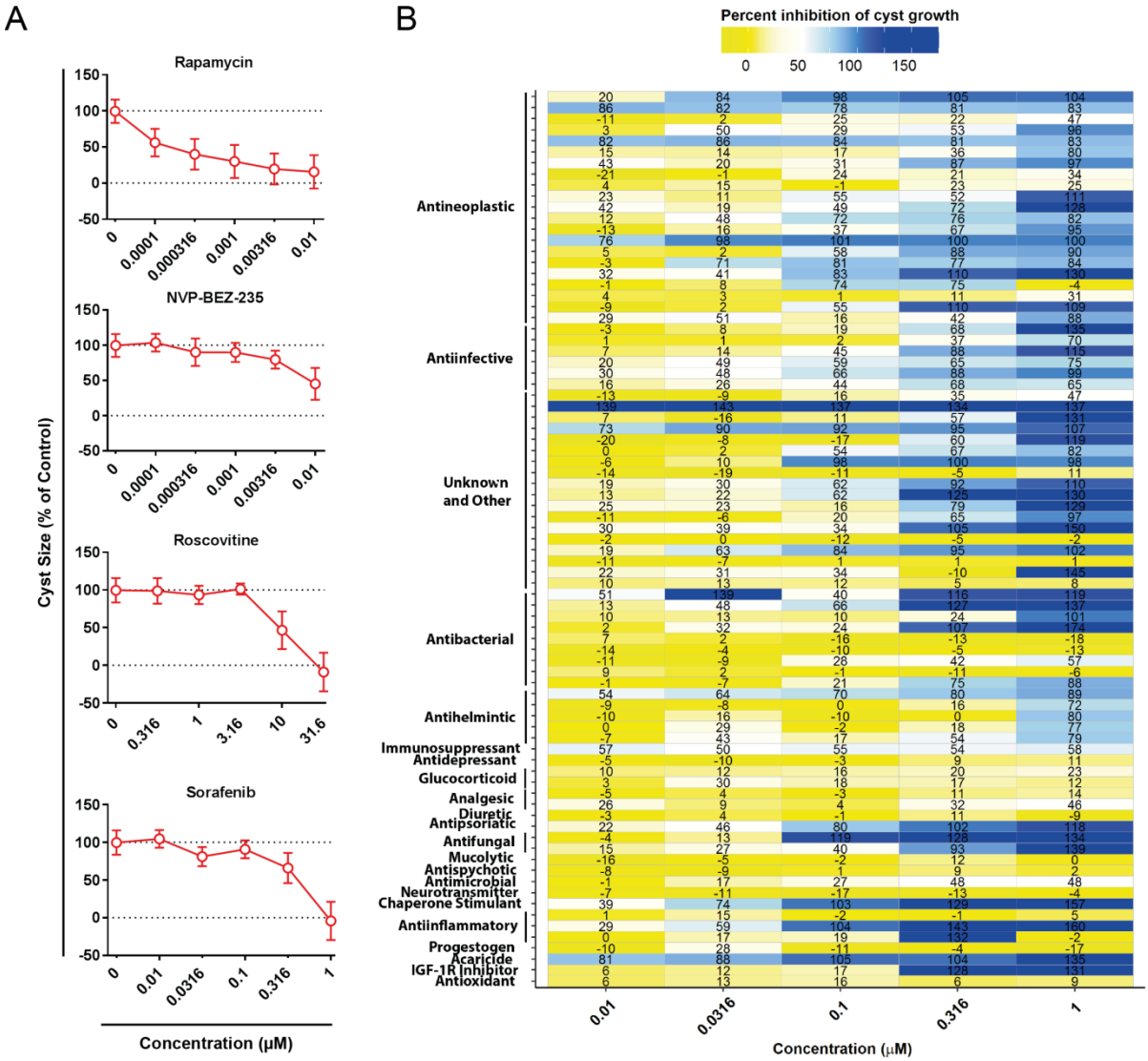

Supplemental figure S2: Screen validation on mIMCD3 Pkd1$^{-/-}$ cysts. A) Concentration-response curves of positive control molecules in the validation screen. Cyst size was scaled to %-cyst growth: 100% represents forskolin-stimulated control (large cysts), 0% represents unstimulated control (small cysts). Means ± SD shown from triplicate wells. B) 81 cyst-growth inhibition molecules rescreened at 5 concentrations. Described bioactivity of the manufacturer's datasheet displayed on y-axis. Potency of molecules represented by percent-inhibition of forskolin-induced cyst growth, as represented by the colour scale and the numbers displayed (means of triplicate wells). 52/81 molecules showed activity >50% inhibition at 1μM concentration.

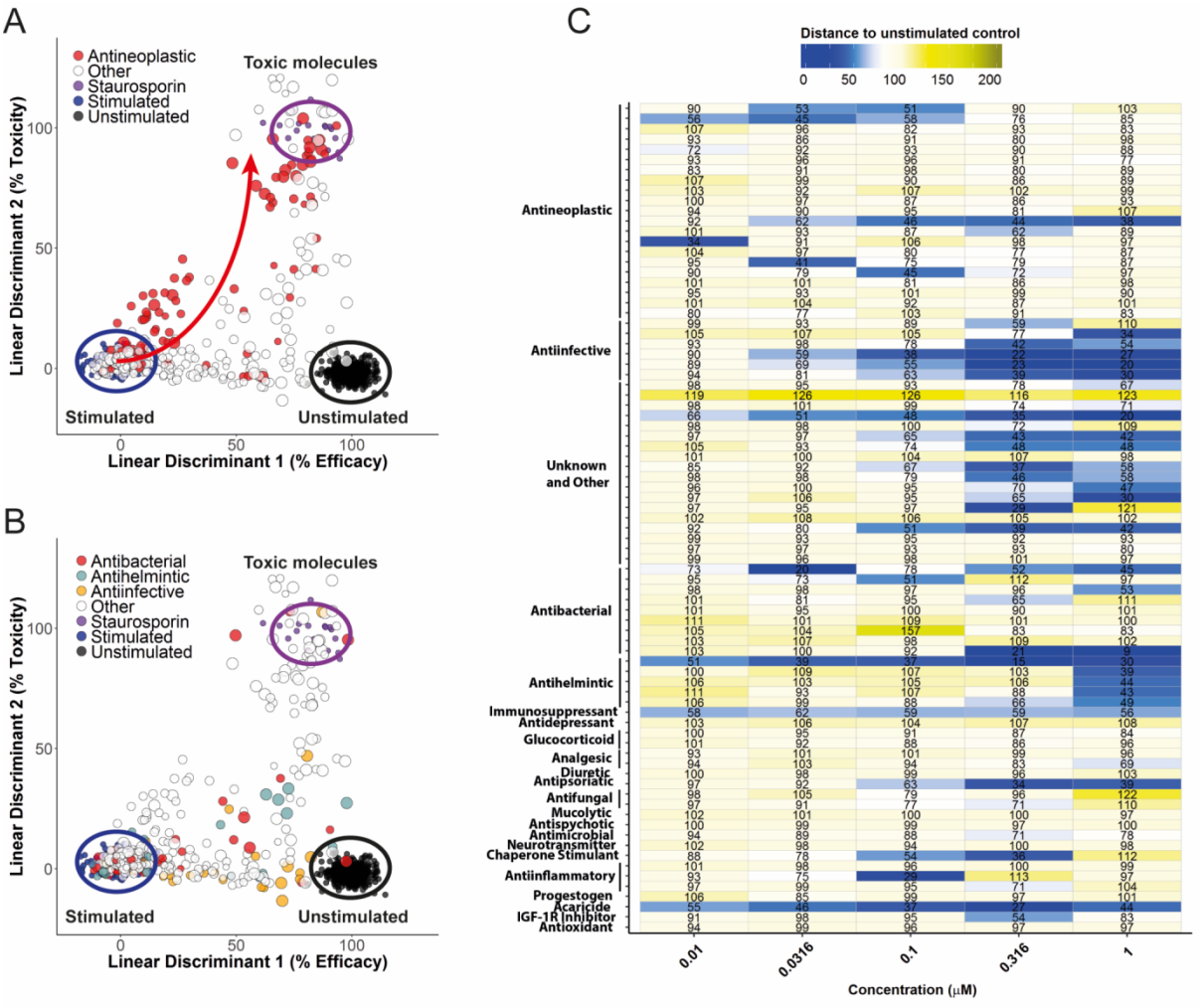

Supplemental figure S3: Linear discriminant analysis discriminates antineoplastic molecules. A-B) LDA was trained as described in supplemental methods (using phenotypic parameters with linear correlation <0.85) and could discriminate antineoplastic molecules (A, red circles) from the unstimulated- and stimulated controls, indicated by black and blue circles, respectively, while retaining activity of others such as antibacterial (B, red circles), antihelmintic (B, light blue) or antiinfective molecules (B, yellow). Point size corresponds with concentration and points shown represent means of triplicate wells (except for "Stimulated", "Unstimulated" and "Staurosporin": individual data points shown). C) Measurement of desirable efficacy -similar to supplemental figure S2B, but presenting absolute distance to unstimulated control calculated from supplemental figure S3B, presented as colour scale and numeric values. Blue colours indicate efficacy.

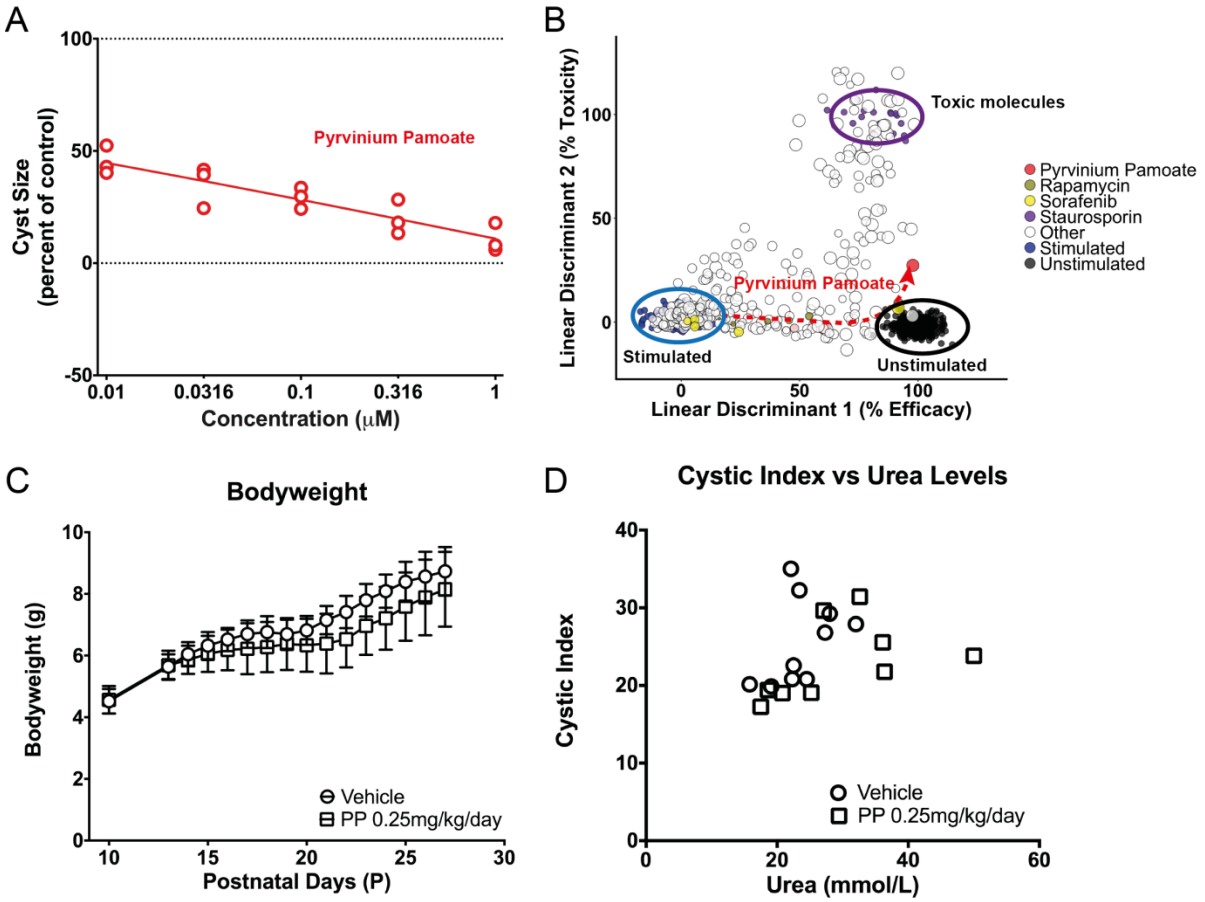

Supplemental figure S4: Pyrvinium pamoate (PP) shows potent efficacy in vitro, but not in vivo. A) PP inhibits forskolin-induced cyst growth of mIMCD3 *Pkd1*$^{-/-}$ cysts (100%, forskolin-stimulated; 0%, unstimulated). Individual wells shown as red circles. B) LDA plot indicates potent desirable efficacy of PP, and indicates no toxic effects. C) In total 17 mice received with PP treatment at postnatal day 13. Ten of those started at 1mg/kg/day of which three mice died within 4-6 days after the start of the treatment. As PP was poorly tolerated at 1mg/kg/day, we reduced the dosage for the 7 remaining mice to 0.25mg/kg/day. In order to obtain sufficient group size, 7 mice were included later during the experiment and were only treated with 0.25mg/kg/day. PP did not affect bodyweight at 0.25mg/kg/day. (vehicle n=11, PP n=14, mean ± SD shown). C) At 0.25mg/kg/day, PP did not lower cystic index or urea levels (vehicle n=10 and PP n=9 shown).

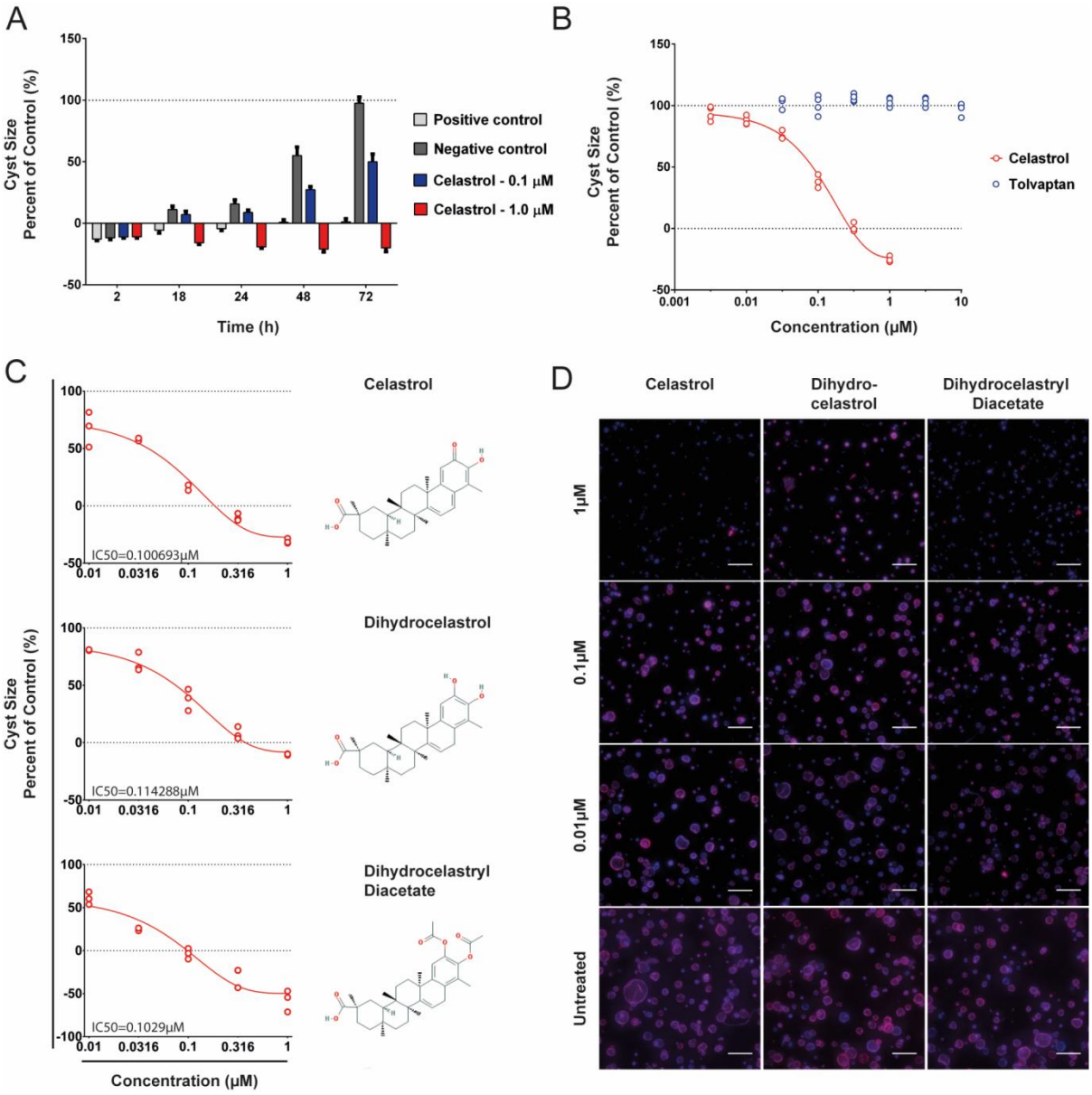

Supplemental figure S5: Inhibition of cystogenesis by celastrol is observed after 48 hours of co-treatment with forskolin and structural analogues of celastrol also potently inhibit forskolin-induced cyst growth in vitro in mIMCD3 Pkd1$^{-/-}$ cysts. A) Inhibitory effects of celastrol at 100nM or 1µM from 48 hours of co-exposure with 2.5µM forskolin. Positive control represents unstimulated condition, negative control represents solvent with 2.5µM forskolin. Cultures were fixed and stained 2, 18, 24, 48 or 72 hours after co-treatment with forskolin and celastrol. Data was normalized to positive- and negative control conditions for presentation purposes. Bars and error bars represent mean and SD of 8 replicates. B) Celastrol inhibits forskolin-induced cyst swelling in mIMCD3 cysts with IC50 around 100nM, whereas tolvaptan does not show effects at concentrations ≤10µM. C) Dihydrocelastrol (middle panel) and dihydrocelastryl diacetate (bottom panel) were included in the molecule library and inhibited forskolin-induced cyst growth similarly to celastrol (top panel). Curve fitting and IC50 calculation performed in GraphPad Prism. Due to residual compound efficacy at the lowest tested concentration the calculated IC50 does not represent 50%

inhibition compared to control condition. Structural formulae shown on the right were obtained from PubChem. D) Representative images of celastrol-treated, dihydrocelastrol-treated or dihydrocelastryl diacetate-treated mIMCD3 *Pkd1*$^{-/-}$ cysts. Images shown are collapsed-stack images of nuclei (Hoechst 33258, blue) and F-actin (rhodamine-phalloidin, red) combined. Images show a 500x500px cut-out from the center of the well. Images were taken with the ImageXpress micro XLS imager. Untreated control condition represents forskolin stimulated controls (corresponding with 100% cyst size in figure C). Scale bars represent 250µm.

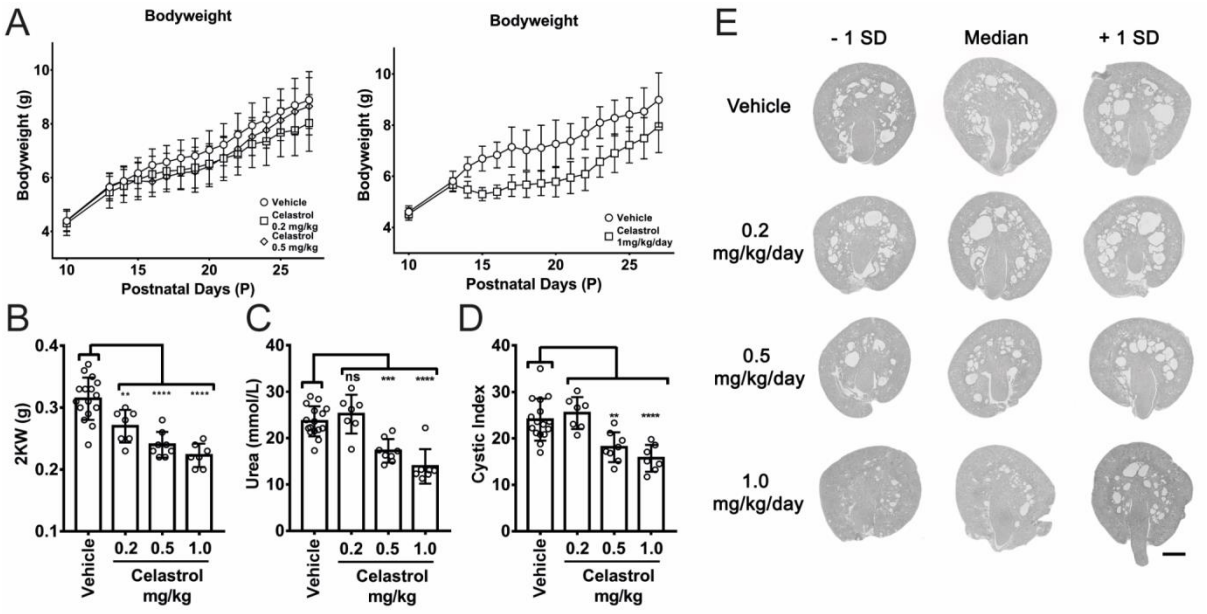

Supplemental figure S6: Celastrol potently inhibits cystogenesis in an in vivo model of PKD. A) Bodyweight is affected by 1mg/kg/day and 0.5mg/kg/day between P13 and P18. B-D) Treatment with 0.5 and 1mg/kg/day celastrol lowers two-kidney weight (B), urea levels (C) and cystic index (D) as compared to vehicle control. For these charts, we pooled the experimental data of two independent experiments (0.2 and 0.5mg/kg/day versus 1mg/kg/day celastrol), because the vehicle controls were highly similar. Mean ± SD as well as individual mice shown. *p<0.05, **p<0.01, ***p<0.001, ****p<0.0001 with ordinary one-way ANOVA with Dunnett's multiple comparison's test. E) Histology reveals that celastrol potently inhibited cyst growth at 0.5 and 1mg/kg/day. Images displaying cystic index close to median ±1SD were selected and presented here.

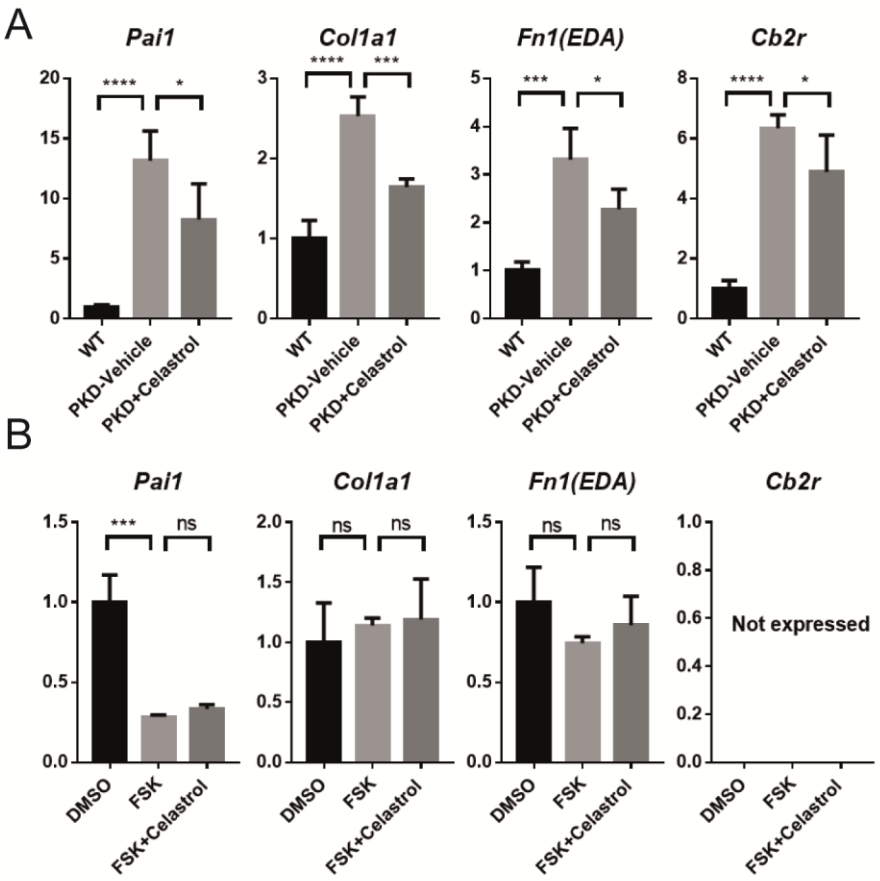

Supplemental Figure S7: Gene expression of Smad2/3 target genes and Cb2R in 3D cysts and in mice. A) relative expression of the Smad2/3 targets *Pai1*, *Col1a1* and *Fn1(EDA)*, as well as expression of *Cb2r* in wild-type mice, PKD mice, and PKD mice treated with celastrol. Potential differences were tested between WT vs PKD-vehicle, and PKD-vehicle vs PKD-celastrol with ANOVA corrected for multiple testing using Dunnett's multiple correction test. B) Relative expression of the same genes in 3D-cysts treated with DMSO, FSK of FSK-celastrol. Potential differences were tested between DMSO vs FSK, and FSK vs FSK-celastrol with ANOVA corrected for multiple testing using Dunnett's multiple correction test. (FSK, forskolin).

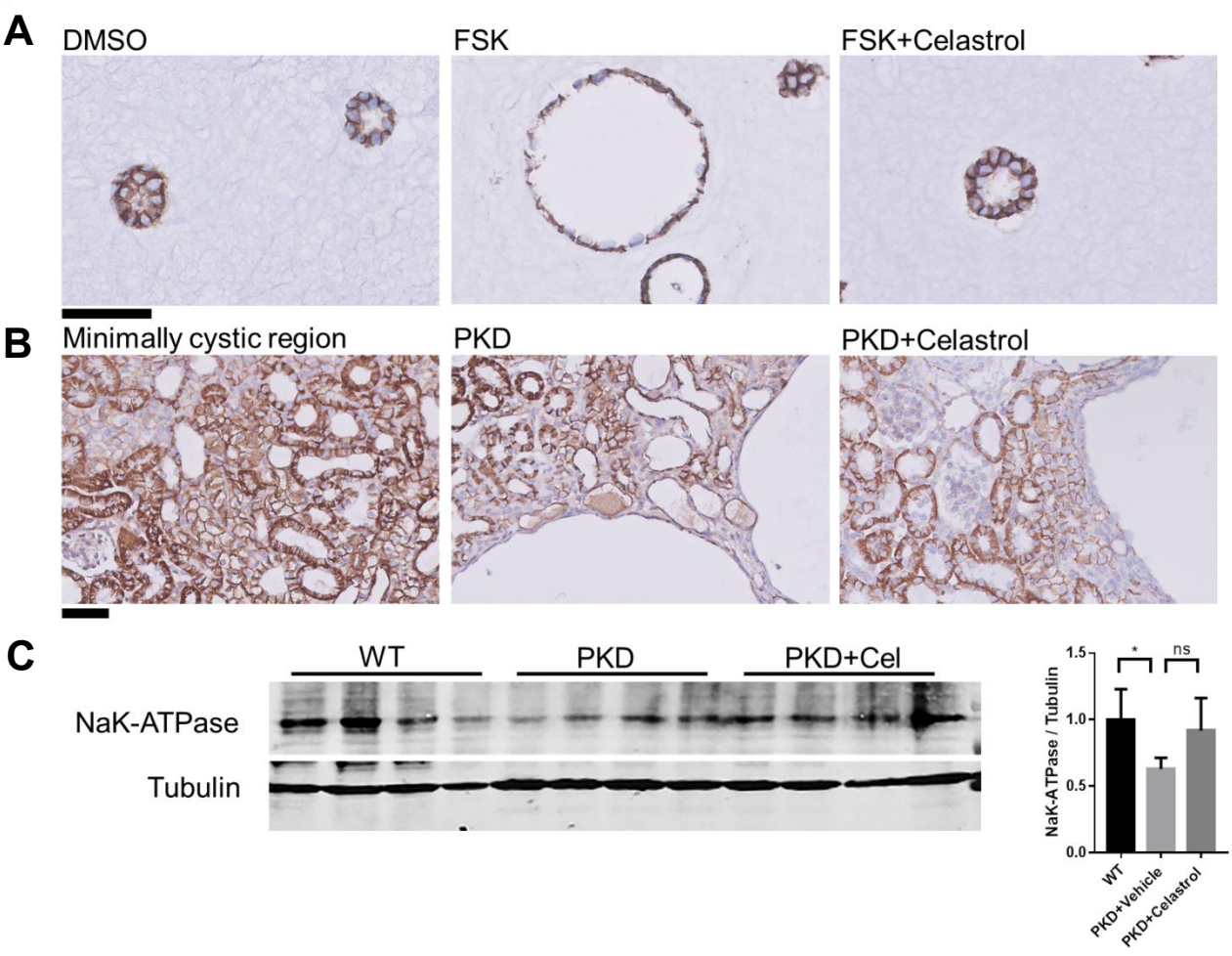

Supplemental figure S8: Celastrol does not significantly alter subcellular Na^+/K^+-ATPase expression. A, B) Immuno-histochemistry with anti-Na^+/K^+-ATPase on sections of 3D-cyst cultures with and without forskolin (scale bar 50µm) (A) and on P10-PKD mice (B), treated with- or without celastrol (scale bar 50µm) .Note that the expression of Na^+/K^+-ATPase in cystic epithelia of mice appears to be lower than in healthy tubules. C) Representative western blot containing samples of kidneys from WT, PKD-vehicle or PKD-celastrol treated mice, hybridized with anti- Na^+/K^+-ATPase (~100 kDa) (left). Densitometry of tubulin and Na^+/K^+-ATPase signals from 5 different blots were used to calculate the relative Na^+/K^+-ATPase protein expression (right). Potential differences were tested between WT vs PKD-vehicle, and PKD-vehicle vs PKD-celastrol with ANOVA corrected for multiple testing using Dunnett's multiple correction test. Western blotting confirms lower Na^+/K^+-ATPase expression in PKD mice. The expression of Na^+/K^+-ATPase in celastrol treated mice appears to becomparable to wt mice, which may be explained by the lower cystic load in these animals compared to the PKD mice. However, the pattern of Na^+/K^+-ATPase expression is not different in celastrol treated PKD mice compared to vehicle treated PKD mice (B). (FSK, forskolin; Cel, celastrol).

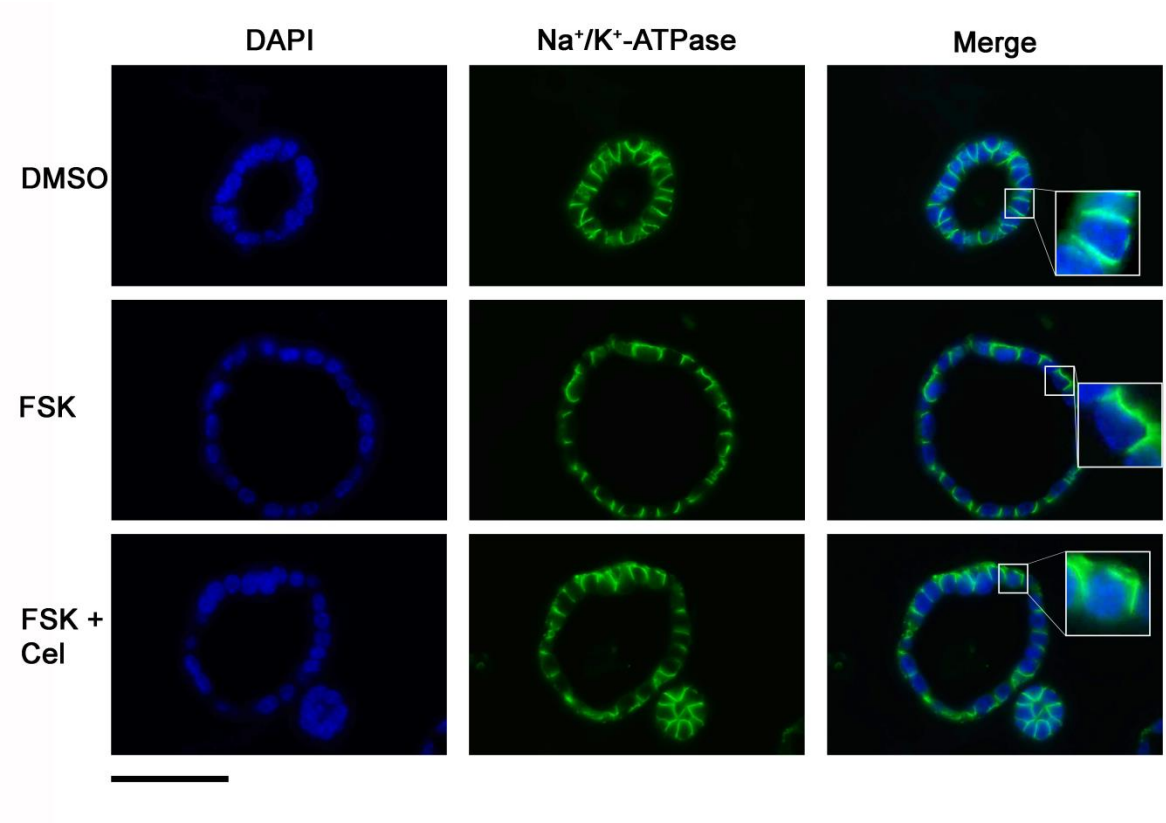

Supplemental figure S9: Fluorescent immunohistochemistry confirms that Celastrol does not affect subcellular localization of Na^+/K^+-ATPase. Shown are images of fluorescent immunohistochemistry with anti-Na^+/K^+-ATPase and DAPI nuclear staining (DAPI in bleu, Na^+/K^+-ATPase in green, and merged on the right side) on sections of 3D-cyst cultures treated without forskolin (DMSO control), with forskolin (FSK) or with forskolin and 100 nM Celastrol (FSK + Cel). In the merged images also a magnified region is shown. Na^+/K^+-ATPase appears to be expressed at the lateral, and to lesser extent at the basal membrane, but not at the apical side. The subcellular localization of Na^+/K^+-ATPase does not differ between FSK and FSK+Celastrol treated 3D-cysts (scale bar 50µm).